June 16, 2017

Microarray analysis of aging-associated immune system alterations in the rostral ventrolateral medulla of F344 rats

Sivasai Balivada, *University of Texas at El Paso*
Chanran K Ganta, *Kansas State University*
Yongqing Zhang, *University of Texas at El Paso*
Hitesh N Pawar, *University of Texas at El Paso*
Richard J Ortiz, *University of Texas at El Paso*, et al.

Physiol Genomics 49: 400–415, 2017.
First published June 16, 2017; doi:10.1152/physiolgenomics.00131.2016.

RESEARCH ARTICLE | *Physiological and Genetic Control of Neural Function*

Microarray analysis of aging-associated immune system alterations in the rostral ventrolateral medulla of F344 rats

Sivasai Balivada,[1]* Chanran K. Ganta,[2]* Yongqing Zhang,[3] Hitesh N. Pawar,[1] Richard J. Ortiz,[1] Kevin G. Becker,[3] Arshad M. Khan,[1] and Michael J. Kenney[1]

[1]*Department of Biological Sciences, College of Science, University of Texas at El Paso, El Paso, Texas;* [2]*Department of Diagnostic Medicine/Pathobiology, Kansas State University, Manhattan, Kansas; and* [3]*Gene Expression and Genomics Unit, National Institute on Aging, Baltimore, Maryland*

Submitted 20 December 2016; accepted in final form 12 June 2017

Balivada S, Ganta CK, Zhang Y, Pawar HN, Ortiz RJ, Becker KG, Khan AM, Kenney MJ. Microarray analysis of aging-associated immune system alterations in the rostral ventrolateral medulla of F344 rats. *Physiol Genomics* 49: 400–415, 2017. First published June 16, 2017; doi:10.1152/physiolgenomics.00131.2016.—The rostral ventrolateral medulla (RVLM) is an area of the brain stem that contains diverse neural substrates that are involved in systems critical for physiological function. There is evidence that aging affects some neural substrates within the RVLM, although age-related changes in RVLM molecular mechanisms are not well established. The goal of the present study was to characterize the transcriptomic profile of the aging RVLM and to test the hypothesis that aging is associated with altered gene expression in the RVLM, with an emphasis on immune system associated gene transcripts. RVLM tissue punches from young, middle-aged, and aged F344 rats were analyzed with Agilent's whole rat genome microarray. The RVLM gene expression profile varied with age, and an association between chronological age and specific RVLM gene expression patterns was observed [$P < 0.05$, false discovery rate (FDR) < 0.3]. Functional analysis of RVLM microarray data via gene ontology profiling and pathway analysis identified upregulation of genes associated with immune- and stress-related responses and downregulation of genes associated with lipid biosynthesis and neurotransmission in aged compared with middle-aged and young rats. Differentially expressed genes associated with the complement system and microglial cells were further validated by quantitative PCR with separate RVLM samples ($P < 0.05$, FDR $<$ 0.1). The present results have identified age-related changes in the transcriptomic profile of the RVLM, modifications that may provide the molecular backdrop for understanding age-dependent changes in physiological regulation.

aging; rostral ventrolateral medulla; transcriptomics; neuro-immunology, microarrays

THE ROSTRAL VENTROLATERAL MEDULLA (RVLM) is an important division of the brain stem that contains diverse neural substrates that are involved in neural systems critical for survival, including those serving respiratory, cardiovascular, metabolic sensing, and visceromotor functions (8, 37, 38). Originally defined on the basis of its observed functional role in increasing arterial blood pressure when stimulated, and less precisely on the basis of anatomical criteria per se (50), the RVLM is now well characterized as harboring neurons that display distinct morphological (35), electrophysiological (34), chemoarchitectural (54), and connectional (9, 10, 14) profiles that do not readily lend themselves to classification within discrete regions on the basis of cytoarchitecture alone (8, 49). Despite our relatively coarse understanding of the locations of these diverse neuronal populations within the RVLM, there remains much attention in clinical circles that this region contains important neural substrates whose dysfunction may be linked to key disease states associated with nutrient sensing, viscerosensation, and sympathetic nervous system (SNS) regulation (5, 11, 58, 64). However, whether specific molecular expression patterns change within the RVLM in relation to these disease states remains largely unknown, nor is it clear whether such patterns coincide with the normal development of these systems across time, such as during aging.

We are interested in how aging, and the heightened immune reactivity in the brain that accompanies aging (6, 17, 18, 20, 23, 32, 39, 61), affects RVLM-related systems in general and RVLM neuronal populations regulating the SNS in particular. There is evidence that aging affects some neural substrates within and connected to the RVLM that influence respiratory and cardiovascular function (43, 55) and also SNS regulation (24).

However, whether advanced age alters the molecular mechanisms of this critical brain-stem area remains unknown. Accordingly, we reasoned that determining global, age-associated changes in RVLM gene expression would be a useful step toward obtaining a molecular framework for determining mechanisms associated with age-dependent alterations in the critical subsystems served by RVLM neural substrates, including neuronal populations that regulate sympathetic discharge, nutrient sensing, cardiovascular, and respiratory or other critical functions. There remain many unsolved challenges for ensuring that any specific subsystem within the RVLM can be reliably and reproducibly sampled given the coarse understanding of RVLM subregional anatomy. Therefore, determining if aging-associated gene expression changes cut across multiple cell types and subregions of the RVLM may facilitate the understanding of associations between aging and RVLM-related disease states.

The goals of this study were to characterize the global transcriptomic profile of the aging RVLM and to test the hypothesis that aging is associated with altered gene expression in the RVLM with an emphasis on immune system associated

* S. Balivada and C. K. Ganta contributed equally to this work.

Address for reprint requests and other correspondence: S. Balivada, Dept. of Biological Sciences, Rm. 4.216, Univ. of Texas at El Paso, El Paso, TX 79968 (e-mail: sbalivada@utep.edu).

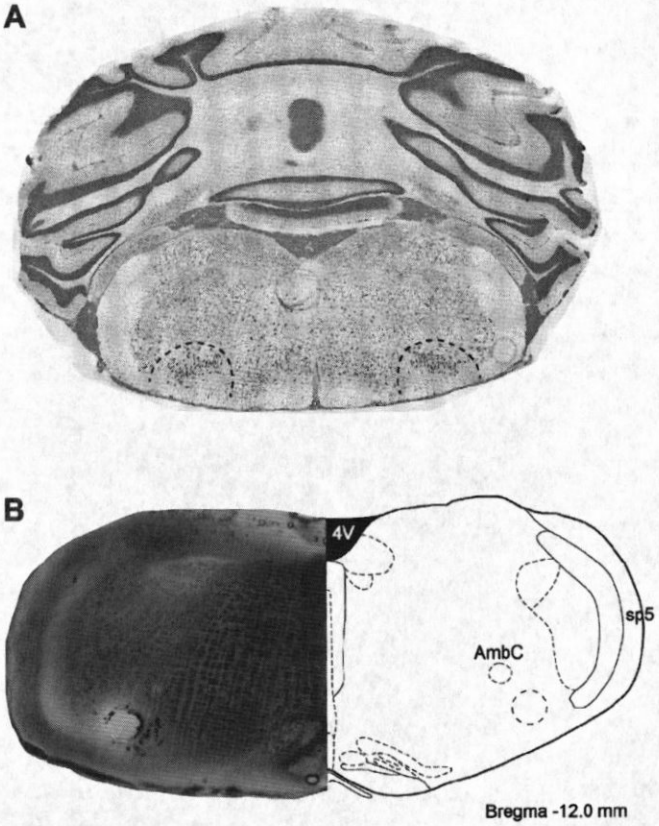

Fig. 1. Validation of the rostral ventrolateral medulla (RVLM) micropunch method. *A*: representative image of a cresyl violet-stained hindbrain section, rostral to the punched sections showing presence of the facial nucleus (marked with dashed lines) (rostrocaudal confirmation). *B*: bright-field image of micropunched brain-stem section showing the location of the punched area relative to other landmarks (dorsoventral confirmation). 4V; 4th ventricle, AmbC; nucleus ambiguus, compact part; sp5; spinal trigeminal tract.

gene transcripts. Accordingly, brain tissue containing the RVLM was micropunched from young, middle-aged, and aged F344 rat hindbrain sections. Purified RNA samples from RVLM-containing tissue punches were analyzed with Agilent's rat whole genome gene expression arrays. Gene set enrichment analysis (GSEA) with Gene Ontology (GO) and Pathway gene sets on microarray probe values revealed that aging is associated with the upregulation of immune response- and stress response-related genes and a concomitant downregulation of lipid biosynthesis- and chemical neurotransmission-related genes in the RVLM of F344 rats. Age-dependent modifications in immune response genes associated with the complement system and microglia were validated with quantitative (q)PCR from separate RVLM-containing samples.

MATERIALS AND METHODS

Animals and Tissue Collection

All procedures and protocols were approved by the Institutional Animal Care and Use Committees and were completed in accordance with the American Physiological Society's guidelines for research involving animals. Young (3 mo old, 301 ± 20 g), middle-aged (12 mo old, 423 ± 18 g), and aged (24 mo old, 413 ± 20 g) male F344 rats were obtained from Charles River Laboratories (contracted with the National Institute on Aging) and each rat is considered as an experimental unit. F344 rats are a strain of rats provided by the National Institute on Aging for studies focused on aging research and are widely used in this research domain (42). Three-month-old adult rats were considered as young for the purpose of relative age group comparisons and for consistency with previous studies from our laboratory (21, 25, 26). Rats were housed in a conventional housing facility with 0 or 1 cage companions. All the rats were held for more than 1 wk after arrival to allow them to acclimate to their new environment. Rats receiving rat chow and water ad libitum were maintained in a temperature-controlled room at 24°C and on a 12:12 h light-dark cycle. On the day of the tissue harvest, rats were deeply anesthetized with 5% isoflurane followed by decapitation with a guillotine in laboratory conditions (time of day: between 9:00 AM and 4:00 PM). The adequacy of anesthesia was indicated by the absence of a motor response to mechanical stimulation of the hindlimb. Brains were removed within 5 min after decapitation and snap-frozen with liquid nitrogen. All brains were stored at −80°C until use.

RVLM Micropunching Procedure

The stereotaxic coordinate system of the rat brain atlas by Paxinos and Watson (47), along with its photographic documentation of histologically stained hindbrain sections, served as the set of references we used to locate and identify, respectively, the hindbrain region containing the RVLM. This was achieved through two approaches *1*): a priori: before sampling, we used inferred stereotaxic space (28) to perform calibrated sectioning on the basis of stereotaxic boundaries of the RVLM defined by the atlas (Bregma coordinate); and *2*) a posteriori: after sampling, we performed histological analysis to identify cytoarchitectonically demarcated fiducial structures that mark where the rostral pole of the RVLM is not yet present, and then becomes present, within successive tissue sections, as documented histologically by the photomicrographs within the atlas.

A priori approach. Coronal sections of the hindbrain were made through the rostrocaudal extent of the RVLM with a cryostat (Leica CM3050S, Leica Biosystems). Following identification of *lobule 2* of the cerebellar vermis [abbreviated "2Cb"; Fig. 103 of Paxinos and Watson (47)], which served as our rostral fiducial to mark the beginning of calibrated sectioning, ninety 40 μm thick serial sections (~3.6 mm) were obtained and discarded, and then, beginning immediately from the remaining tissue block-face, two serial 200 μm thick coronal sections were collected (beginning at an inferred distance from Bregma of −12.0 mm, or approximately at Fig. 133 of Paxinos

Table 1. *List of immune system genes used for quantitative PCR validation of microarray analysis and their TaqMan assay IDs*

Functional Category	Gene Symbol	TaqMan Assay ID
Complement system	*C1qa*	Rn01519903_m1
	C1qc(C1qg)	Rn01516757_m1
	Cd93(C1qr1)	Rn00584525_g1
	C3	Rn00584525_g1
	C4a	Rn00566466_m1
	Cfd	Rn00709527_m1
	Cfh	Rn01535436_g1
	Vwf	Rn00590326_m1
	Klkb1	Rn01488161_m1
Microglial cells	*Cd14*	Rn00572656_g1
	Cd68	Rn01495634_g1
	Tlr2	Rn02133647_s1
	Cx3cr1	Rn02134446_s1
	Trem2	Rn01512170_m1
	Fcrl2	Rn01455191_m1
	B2m	Rn00560865_m1
Endogenous controls	*Actb*	Rn00667869_m1
	Hprt1	Rn01527840_m1
	Ldha	Rn00820751_g1
	Rplp1	Rn03467157_gH

and Watson (47), and extending to −12.4 mm from Bregma, or approximately at the level shown in Fig. 136 of the atlas).

Once the tissue sections were obtained, the RVLM-containing area was micropunched bilaterally with a Harris micropunch (inner diameter = 0.5 mm) on a frozen block maintained at −10 to −20°C, using a modification of the Palkovits micropunch technique (45, 46). All four tissue punches from each brain were pooled (tissue volume of ~0.8 mm^3) into an RNase-free centrifuge tube and stored at −80°C until use. To decrease cross-contamination and RNA degradation, the micropunch needle and the freezing block were cleaned with 70% alcohol followed by application of RNaseZap (Ambion).

A posteriori approach. To confirm the accuracy of our a priori approach for identifying our sample area, a fiducial analysis was performed of the tissue using two parameters. First, a tissue section (40 μm thick) rostral to the micropunched sections was collected and stained with cresyl violet to confirm the presence of the various parts of the facial nucleus (which mark the tissue that is situated just outside the rostral pole of the RVLM; i.e., the rostrocaudal level situated between that shown in Figs. 132 and 133 of Paxinos and Watson (47), at Bregma coordinate −11.96 mm). As shown in Fig. 1*A*, the Nissl-stained section shows clearly the location of neurons within this nucleus, and no micropunch is visible. Second, the micropunched sections themselves were examined for the presence of the nucleus ambiguus, which is situated dorsal to the RVLM, and this combination occurs within stained sections at the same rostrocaudal level where the rostral pole of the RVLM has already emerged (at Bregma −12.24 mm) (47). As shown in Fig. 1*B*, the micropunched area is observed just ventral to the nucleus ambiguus, confirming that the tissue sample we obtained contained the RVLM.

RNA Purification and Analysis

Following removal of the RVLM-enriched tissue punches from −80°C storage, RNA from the tissue samples was extracted and purified using RNeasy Lipid Tissue mini kit (Qiagen) with QIAzol Lysis reagent (Qiagen) according to the manufacturer's protocol. The quality and quantity of the RNA used for microarray analysis were tested with the Agilent Bioanalyzer with RNA 6000 nano kit (Agilent Technologies). The RNA integrity number (RIN) for the RNA samples was ≥7. The purity of the RNA samples used for qPCR was estimated using Agilent High Sensitivity RNA ScreenTape System on an Agilent TapeStation (Agilent Technologies) and RNA samples with ≥7 RIN were used for qPCR. The quantity of the RNA samples used for qPCR was estimated using a Qubit RNA HS assay kit on

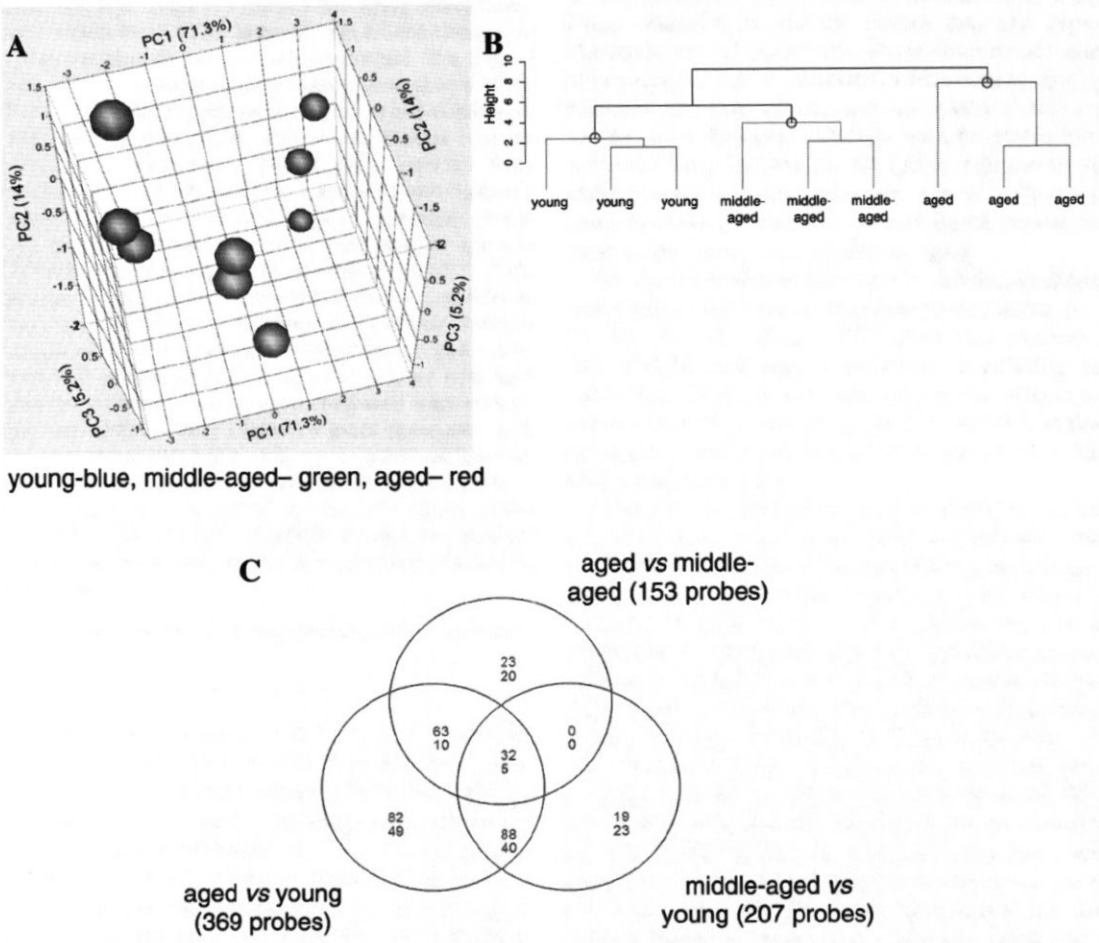

Fig. 2. Unsupervised classification and global differentially expressed (DE) gene comparisons. *A*: principal component analysis (PCA) plot of analyzed young (blue), middle-aged (green), and aged (red) RVLM microarrays (PC1, Principal Component 1; PC2, Principal Component 2; PC3, Principal Component 3). Highest variance was observed between young and aged RVLM microarrays (PC1, 71.3%). *B*: hierarchical clustering dendrogram of microarray sample Z-score values showing intergroup and intragroup relatedness. For each group the vertical distances were marked with a circle. *C*: a Venn diagram showing comparisons between aged vs. young, middle-aged vs. young, and aged vs. middle-aged DE genes. Upregulated genes are in red, and downregulated genes are in blue. The sample size for each group $n = 3$. Statistical criteria for selecting DE genes: ANOVA <0.05, multiple-comparison Z-ratio <−1.5 or >1.5, Z-statistic P value <0.05, false discovery rate (FDR) <0.3, and probe signal intensity >0.

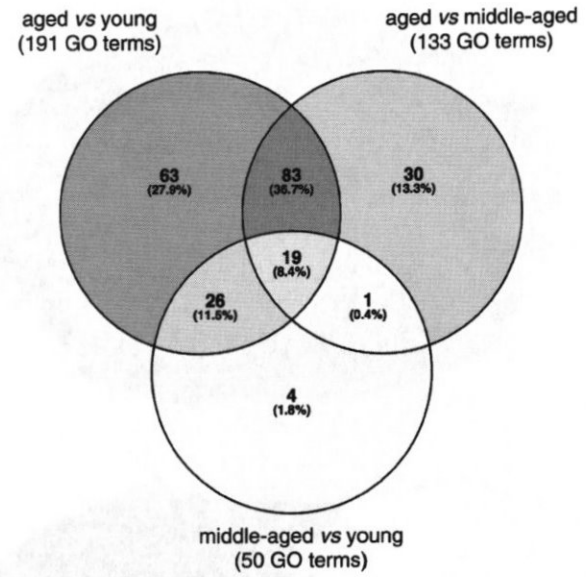

Fig. 3. Relationship between significant Gene Ontology (GO) gene sets identified in aging RVLM gene set enrichment analysis (GSEA). Venn diagram showing relationship between aged vs. young, aged vs. middle-aged, and middle-aged vs. young significant GO gene sets. Subset percentages are represented with increasing background grayscale values.

Qubit Fluorometer (ThermoFisher Scientific) following manufacturer's instructions. Extracted RNA samples were stored at −80°C until use.

Microarray Method

Microarray procedures and analyses were conducted at the Gene Expression and Genomics Unit at the National Institute on Aging (Baltimore, MD). Genome-wide gene expression analysis was performed on young ($n = 3$), middle-aged ($n = 3$), and aged ($n = 3$) RVLM-containing RNA samples by using Agilent's whole rat genome 4x44K microarray kit (product # G413F, design ID-014879, Agilent Technologies). Each array contained 60-mer oligonucleotide probes for 43,379 genes/transcripts and a one-color microarray-based gene expression analysis was conducted according to the manufacturer's instructions. Briefly, 200 ng of total RNA from each sample was labeled with Cy-3 using the Low Input Quick Amp Labeling Kit (product # 5190-2305, Agilent Technologies) following the manufacturer's protocol. The labeled RNA samples were tested for cRNA quantity and Cy-3 specific activity by a NanoDrop ND-1000 UV-vis Spectrophotometer v3.8.1 (Nano Drop Technologies). Labeled samples were hybridized onto the whole rat genome microarray for 17 h at 65°C in a rotator oven, washed following Agilent protocols, and scanned in an Agilent Technologies Array Scanner, G2505A (Agilent Technologies).

qPCR Method

The altered expression of selected immune response-related genes observed in microarray analysis was validated using TaqMan-based qPCR. Ten nanograms of RNA collected from young ($n = 5$), middle-aged ($n = 5$), and aged ($n = 5$) RVLM-containing tissue punches was reverse transcribed to cDNA using a ThermoScript RT-PCR System (ThermoFisher Scientific). The reverse transcription reaction was performed using a Bio-Rad T100 thermal cycler (Bio-Rad) under the following conditions: 25°C (10 min), 50°C (50 min), 85°C (5 min). To increase the number of qPCR reactions from each sample, cDNA was preamplified using TaqMan PreAmp Master Mix (Life Technologies) following manufacturer's instructions. Briefly, 5 μl of cDNA was mixed with 0.2× pooled assay mix containing 20 TaqMan assays (Table 1) and TaqMan PreAmp Master Mix, and pre-amplification was performed using a Bio-Rad T100 thermal cycler under the following conditions: denaturation step at 95°C for 10 min followed by 14 cycles of 95°C (15 s) and 60°C (4 min) steps. qPCR for each gene was performed on these preamplified samples using TaqMan Gene Expression Master Mix on the Step One Plus master cycler (Applied Biosystems) under the following conditions: 50°C (2 min), 95°C (10 min), followed by 40 cycles of 95°C (15 s) and 60°C (1 min). Two technical replicates were conducted for each preamplified sample/gene, and reaction mixes with no template were used as negative controls. *Actb, Hprt1, Ldha*, and *Rplp1* genes were used as endogenous controls and the geometric average of their Ct values was used to calculate each gene's ΔCt value (1).

Microarray Data Analysis

Hybridization signal intensities from microarrays were extracted with Agilent Feature Extraction Software, version 9.5.1.1. (Agilent Technologies) (Gene Expression Omnibus accession number GSE90956). The resulting data set was analyzed with DIANE 6.0, a spreadsheet-based microarray analysis program. By using DIANE, the results were normalized with a Z-Score transformation (12). Z-normalized data were analyzed with principal component analysis (PCA) and unsupervised hierarchal clustering analysis (HCA). To determine the gene expression changes within each specific RNA comparison, Z-scores for paired treatment groups (aged vs. young, middle-aged vs. young, aged vs. middle-aged RVLM) were compared using the Z-Ratio statistic (12). Expression changes for individual genes were considered significant if they met five criteria: ANOVA F-test $P < 0.05$, |Z-ratio| not less than 1.5, false discovery rate (FDR) (56) of < 0.3, a z-test P value statistic for Z-score replicability <0.05; and mean background-corrected signal intensity >0. GSEA for GO was performed using GO gene sets with the PAGE (parametric analysis of gene set enrichment) algorithm (29) as described previously (13). GSEA for canonical pathways was performed using BIOCARTA, KEGG, REACTOME gene sets with the PAGE algorithm (29) as described previously (13). GO or pathway terms with PAGE that have more than three genes for the test gene set (GO or pathway) and a t-test value between the test gene set and whole gene distribution P value <0.05 were considered as significant. GO or pathway terms with positive PAGE Z-score values and more than three genes were interpreted as upregulated, with negative PAGE Z-score values and more than three genes interpreted as downregulated.

Statistical Analysis

Microarray data were analyzed using the JMP12 microarray analysis program and statistical specifications for significance were completed as explained above. PCA plot and differentially expressed (DE) genes' Venn diagrams were constructed using JMP-SAS. GO and Pathway analyses line segment plots were graphed using RStudio with ggplot2 package. GO and pathway terms Venn diagrams were constructed using Venny 2.1.0 online Venn diagram tool (44). Heat maps were constructed using Heatmap builder software (31).

qPCR data were analyzed by taking each sample/gene *base 2* logarithm-transformed $2^{-\Delta Ct}$ value as a parameter (1). Expression changes for individual genes were considered significant if they met three criteria: ANOVA P value <0.05, Benjamini-Hochberg FDR <0.1, and least significant difference post hoc test P value <0.05. Shapiro-Wilk normality test and equal variance test were used to asses ANOVA assumptions. Aged vs. young, aged vs. middle-aged, and middle-aged vs. young rats RVLM gene expression differences are represented as fold change values calculated using the $2^{-\Delta\Delta Ct}$ method (36). Correlation between tested genes microarray and qPCR fold change values was analyzed by calculating the coefficient of determination (r^2) in RStudio. Graphs were plotted in RStudio with ggplot2 package.

RESULTS

Microarray Analysis and DE Genes Comparison

Normalized microarray probe values derived from RVLM-containing samples [young (n = 3), middle-aged (n = 3), aged (n = 3)] were analyzed with PCA and unsupervised HCA to confirm array quality and sample level variances. The PCA plot shown in Fig. 2*A* demonstrates that the largest amount of data variation was observed between young and aged RVLM-enriched microarrays [Principal Component 1 (PC1)–71.3%], with the microarrays from middle-aged rats located in between those of young and aged rats. The relative position of the microarrays in the PCA plot indicates a higher correlation in intragroup than intergroup arrays. Similar relative comparisons were observed in the response patterns shown in the HCA dendrogram (Fig. 2*B*); that is, the discrete vertical distance for each age group (Fig. 2*B*, age group vertical distances were marked with circle).

To determine the presence of age-associated DE genes in RVLM, age groups were analyzed with aged vs. young, middle-aged vs. young, and aged vs. middle-aged multiple comparisons. Results are shown as a Venn diagram in Fig. 2*C*; upregulated genes are colored red and downregulated genes are colored blue. The highest number of DE genes was observed in the aged vs. young (369 probes) comparison, followed by the middle-aged vs. young (207 probes), and aged vs. middle-aged (153 probes) comparisons. The percentage of upregulated genes vs. downregulated genes as of total DE genes was higher in all three comparisons; aged vs. young (71.9%), middle-aged vs. young (67.1%), and aged vs. middle-aged

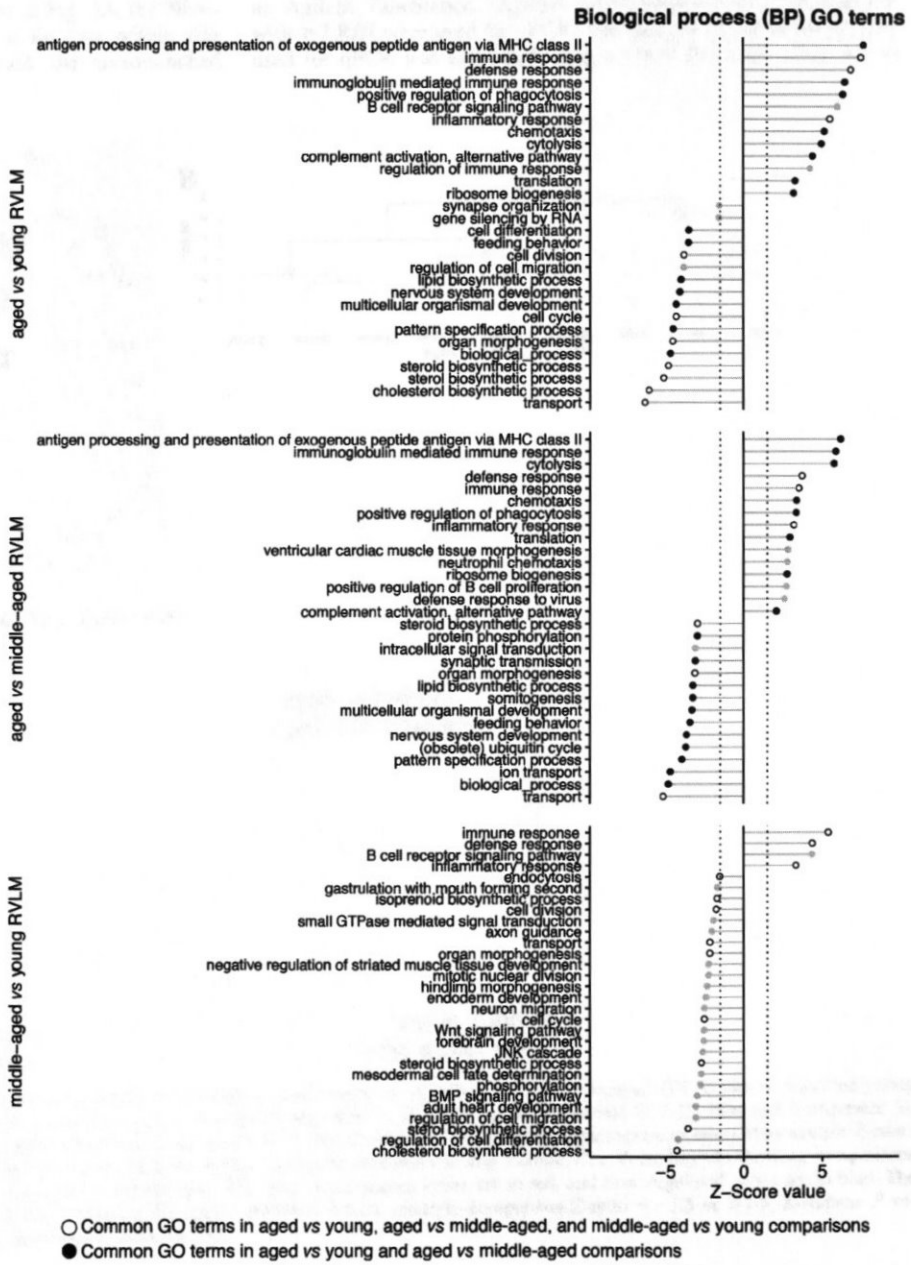

Fig. 4. Comparison of biological process (BP) GO terms in aging RVLM. Horizontal line segment plots of significant top 30 ± Z-score BP GO terms identified in aged vs. young, aged vs. middle-aged, and middle-aged vs. young RVLM GSEA. GO terms with parametric analysis of gene set enrichment (PAGE) Z-score <-1.5 or >1.5 (dotted reference lines on plots) with P values <0.05 were considered as significant. GO term with positive Z-scores and >3 specific genes were considered as upregulated, and GO terms with negative Z-scores and >3 specific genes were considered as downregulated. Horizontal line segments with empty circles represent GO terms that were present in all 3 comparisons; horizontal line segments with black circles represent GO terms that were present in aged vs. young and aged vs. middle-aged comparisons. The sample size for each group n = 3.

(77.1%) (Fig. 2*C*). DE genes identified in the aged vs. young comparison were more common with DE genes identified in middle-aged vs. young, than in the aged vs. middle-aged comparison (Fig. 2*C* Venn diagram, aged vs. young ∩ middle-aged vs. young-165 probes, aged vs. young ∩ aged vs. middle-aged-110 probes).

Aging RVLM GO Analysis and Comparison of GO Terms

To characterize the ontological profile of the aging RVLM-containing samples, microarray probe Z-score values were compared between age groups using PAGE- based GSEA [young (n = 3), middle-aged (n = 3), aged (n = 3)]. To illustrate age-dependent GO changes in the RVLM, relationships between significant GO terms identified in aged vs. young, aged vs. middle-aged, and middle-aged vs. young RVLM comparisons are represented with a Venn diagram in Fig. 3. The aged vs. young comparison yielded the highest number of significant GO terms (191 terms, 84.5% in GO terms identified in all three comparisons) followed by aged vs. middle-aged (133 GO terms, 58.8% in GO terms identified in all three comparisons) and middle-aged vs. young comparisons (50 GO terms, 22.1% in GO terms identified in all three comparisons) (Fig. 3, Supplemental File 1). (The online version of this article contains supplemental material.) The top 30 ± PAGE Z-score significant GO terms identified in biological process (BP), cellular component (CC), molecular function (MF) GO domains describing aged vs. young, aged vs. middle-aged, and middle-aged vs. young comparisons are represented

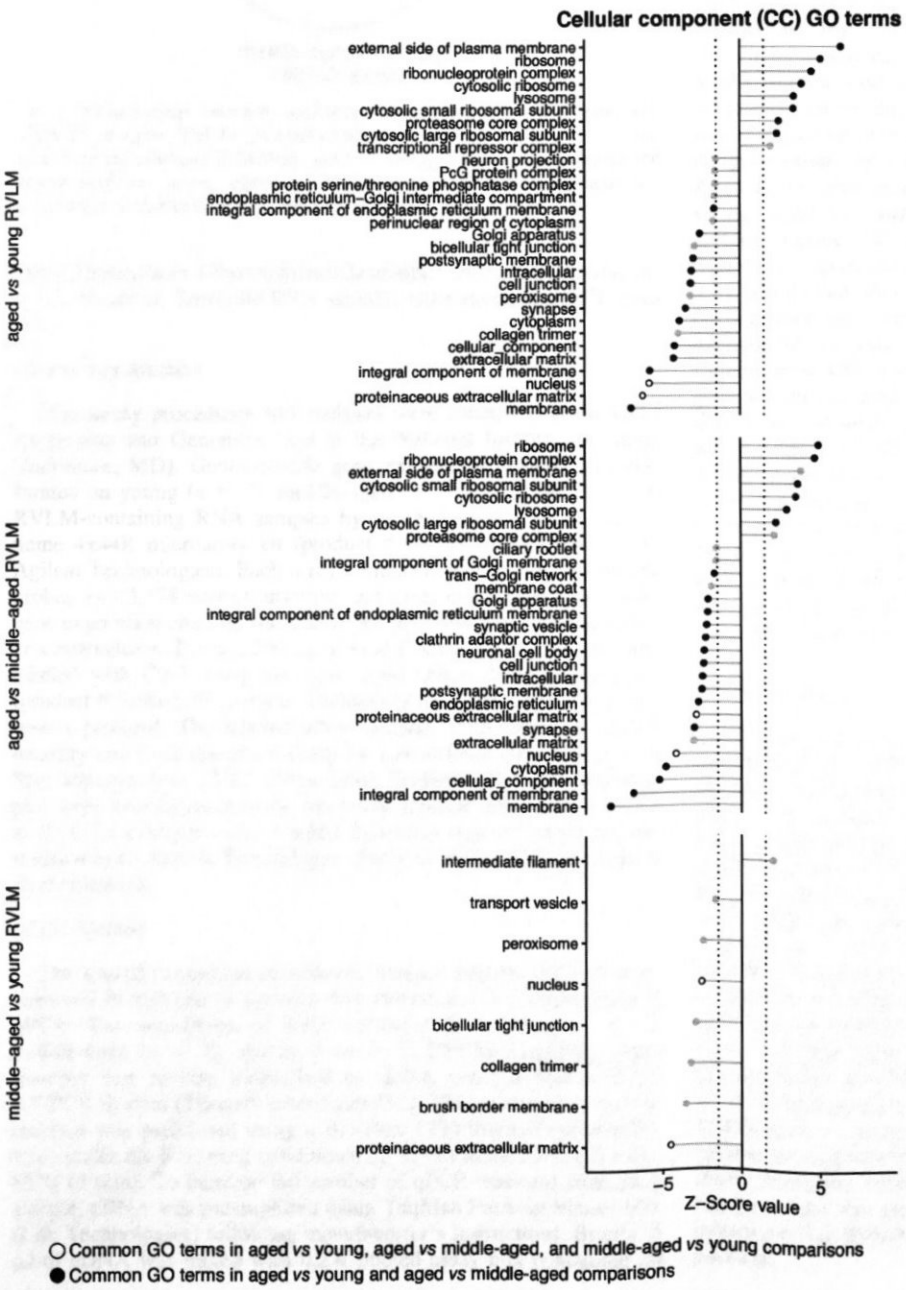

Fig. 5. Comparison of cellular component (CC) GO terms in aging RVLM. Horizontal line segment plots of significant top 30 ± Z-score CC GO terms identified in aged vs. young, aged vs. middle-aged, and middle-aged vs. young RVLM GSEA. GO terms with PAGE Z-score <-1.5 or >1.5 (dotted reference lines on plots) with P values <0.05 were considered as significant. GO term with positive Z-scores and >3 specific genes were considered as upregulated, and GO terms with negative Z-scores and >3 specific genes were considered as downregulated. Horizontal line segments with empty circles represent GO terms that were present in all 3 comparisons; horizontal line segments with black circles represent GO terms that were present in aged vs. young and aged vs. middle-aged comparisons. The sample size for each group n = 3.

as horizontal line segment plots in Figs. 4–6. Nineteen significant GO terms were common in all three comparisons (Fig. 3, Supplemental File 1). Significantly upregulated BP GO terms that were common in all three comparisons were associated with an "immune system process" and "response to stress" GO hierarchy ("immune response," "defense response," "inflammatory response") (Fig. 4). In MF domain, the "endopeptidase inhibitor activity" GO term was significantly upregulated in all three comparisons (Fig. 6). Significantly downregulated BP GO terms that were common in all three comparisons were associated with "lipid biosynthetic process," "organ morphogenesis," and "transport" GO hierarchy (Fig. 4, Supplemental File 1). "extracellular matrix, nucleus" GO branch associated CC GO terms (Fig. 5, Supplemental File 1) and "nucleic acid binding, transporter activity" MF GO terms were identified as downregulated in all three comparisons (Fig. 6, Supplemental File 1).

GO terms identified in aged vs. young GSEA were more common with GO terms identified in aged vs. middle-aged, than in middle-aged vs. young comparisons (Fig. 3, aged vs. young ∩ aged vs. middle-aged, 45.1%; aged vs. young ∩ middle-aged vs. young, 19.9% GO terms). A total of 102 common significant GO terms were present in aged vs. young and aged vs. middle-aged comparisons (Fig. 3). GO terms related to innate and adaptive immune responses like "positive regulation of phagocytosis," "antigen processing and presentation of exogenous peptide antigen via MHC class II," "immunoglobulin mediated immune response," and "complement activation alternative pathway" were observed to be upregulated in aged vs. young and aged vs. middle-aged comparisons

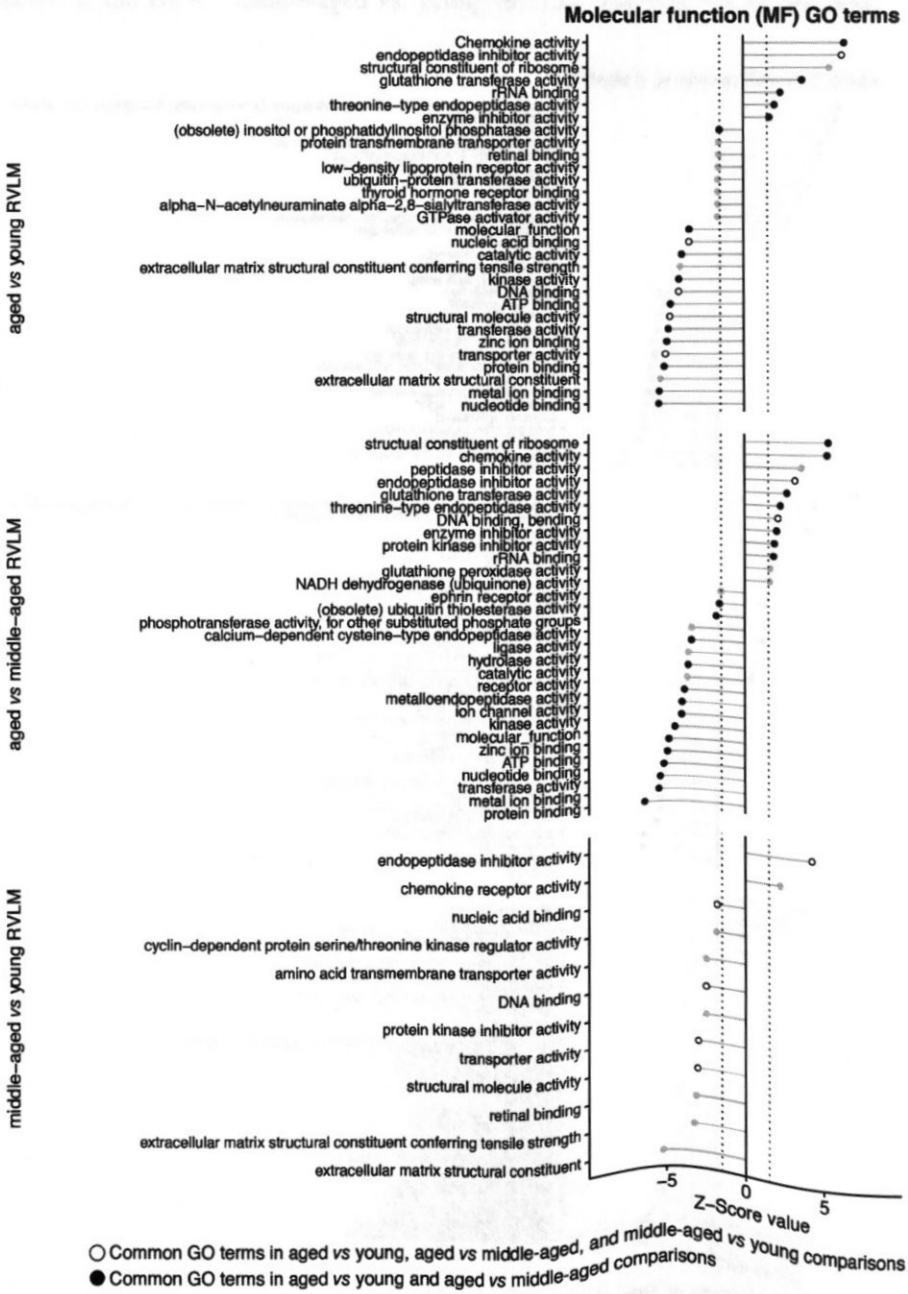

Fig. 6. Comparison of molecular function (MF) GO terms in aging RVLM. Horizontal line segment plots of significant top 30 ± Z-score MF GO terms identified in aged vs. young, aged vs. middle-aged, and middle-aged vs. young RVLM GSEA. GO terms with PAGE Z-score <-1.5 or >1.5 (dotted reference lines on plots) with P values <0.05 were considered as significant. GO term with positive Z-scores and >3 specific genes were considered as upregulated, and GO terms with negative Z-scores and >3 specific genes were considered as downregulated. Horizontal line segments with empty circles represent GO terms that were present in all 3 comparisons; horizontal line segments with black circles represent GO terms that were present in aged vs. young and aged vs. middle-aged comparisons. The sample size for each group $n = 3$.

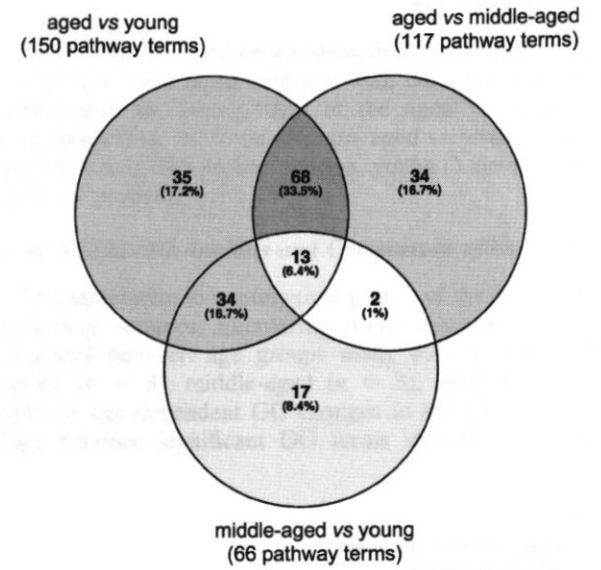

Fig. 7. Relationship between significant pathway gene sets identified in aging RVLM GSEA. Venn diagram showing relationship between aged vs. young, aged vs. middle-aged, and middle-aged vs. young significant pathway gene sets. Subset percentages are represented with increasing background grayscale values.

(Fig. 4). Immune- and stress response-related MF GO terms such as "chemokine activity" and "glutathione transferase activity" were upregulated in these two comparisons (Fig. 6). Apart from these sets, CC GO terms associated with protein translation and degradation were significantly upregulated (Fig. 5). Intermolecular binding MF- related GO terms were downregulated significantly in aged vs. young and aged vs. middle-aged comparisons (Fig. 6). Neurotransmission-related GO terms like "synapse," "synaptic transmission," "synaptic vesicle," "post synaptic membrane" and "ionotropic glutamate receptor activity" were present in aged vs. young and aged vs. middle-aged comparisons downregulated GO terms (Supplemental File 1).

Aging RVLM Pathway Analysis and Comparison of Pathway Terms

Altered RVLM canonical pathways were identified through GSEA between young (n = 3), middle-aged (n = 3), and aged (n = 3) F344 rats RVLM microarrays. To illustrate age-dependent changes in biological pathways in the RVLM, relationships between significant canonical pathway terms identified in aged vs. young, aged vs. middle-aged, and middle-aged vs. young RVLM comparisons are represented with a Venn diagram in Fig. 7. Aged vs. young RVLM GSEA analysis yielded the highest number significantly altered canonical pathway terms (150 terms) followed by aged vs. middle-aged (117 terms) and middle-aged vs. young (66 terms) (Fig. 7, Supplemental File 2). For aged vs. young, aged vs. middle-aged and middle-aged vs. young comparisons, the significant top 30 ± PAGE Z-score GO terms were represented as horizontal line segment plots in Figs. 8–10. Significantly altered pathway terms that were common in all three comparisons (Fig. 7; 13 pathway terms, 6.4% in pathway terms identified in all three comparisons) were associated with immune system regulatory functions and lipid metabolism (Figs. 8–10, Supplemental File 2). In all three comparisons, the majority of the genes related to immune system regulatory pathways were upregulated and genes related to lipid metabolic pathways were downregulated. The "reactome immunoregulatory interactions between a lymphoid and a non-lymphoid cell" pathway term was present in all three comparisons as designated by a high absolute Z-score value (Figs. 8–10, |Z-score| >5, P value <0.05, FDR <0.3). Similar to GO analysis, pathways terms related to innate and adaptive immune responses like "reactome initial triggering of complement," "KEGG complement and coagulation cascades," "Biocarta CTL pathway," and "reactome signaling in immune system" were present in all three comparisons (Figs. 8–10). Lipid metabolism-related pathway terms, such as "reactome cholesterol biosynthesis," "reactome steroid metabolism," "reactome transformation of lanosterol to cholesterol," "KEGG steroid biosynthesis," and "KEGG terpenoid biosynthesis," and the neuroplasticity-related pathway term, "reactome NCAM signaling for neurite out growth," were present in all three comparisons with downregulated genes. Immune system- and lipid biosynthesis-related DE genes are represented as a heat map in Fig. 11.

Pathway terms identified in aged vs. young GSEA were more common with pathway terms identified in aged vs. middle-aged comparisons, than in middle-aged vs. young (Fig. 7, aged vs. young ∩ aged vs. middle-aged- 39.9%, aged vs. young ∩ middle-aged vs. young, 23.1% pathway terms). A total of 81 common significant pathway terms were present in aged vs. young and aged vs. middle-aged comparisons (Fig. 7). Apart from immune and lipid pathways, neurotransmission- and protein metabolism-related pathways were identified as significant in aged vs. young and aged vs. middle-aged RVLM GSEA (Figs. 8 and 9). Chemical neurotransmission pathways that can effect RVLM function, such as "reactome neurotransmitter release cycle," "KEGG neuroactive ligand receptor interaction," "reactome transmission across chemical synapses," "KEGG axon guidance," "reactome transmembrane transport of small molecules," and the "KEGG calcium signaling pathway" were significant in aged vs. young and aged vs. middle-aged RVLM GSEA analysis. Genes associated with these pathways were downregulated in the RVLM of aged rats.

qPCR Validation of Aging RVLM Immune Response Genes' Differential Expression

To validate the microarray results, we selected 16 genes based on two selection criteria. Genes that belong to the "immune response" GO term as well as several pathway terms (e.g., "reactome immunoregulatory interactions between a lymphoid and a non-lymphoid cell," "reactome initial triggering of complement," and "KEGG complement and coagulation cascades") and DE genes that were significant with the five statistical criteria identified in MATERIALS AND METHODS. These 16 genes were categorized into complement system and microglial cell associated genes based on the extant literature and tabulated in Table 1. Expression differences observed through qPCR for these genes in all three comparisons are shown in Fig. 12 as relative mean fold change values with their standard error [young (n = 5), middle-aged (n = 5), aged (n = 5)]. For direct comparisons, fold change values identified by microarray were also plotted in Fig. 12. Similar expression differences

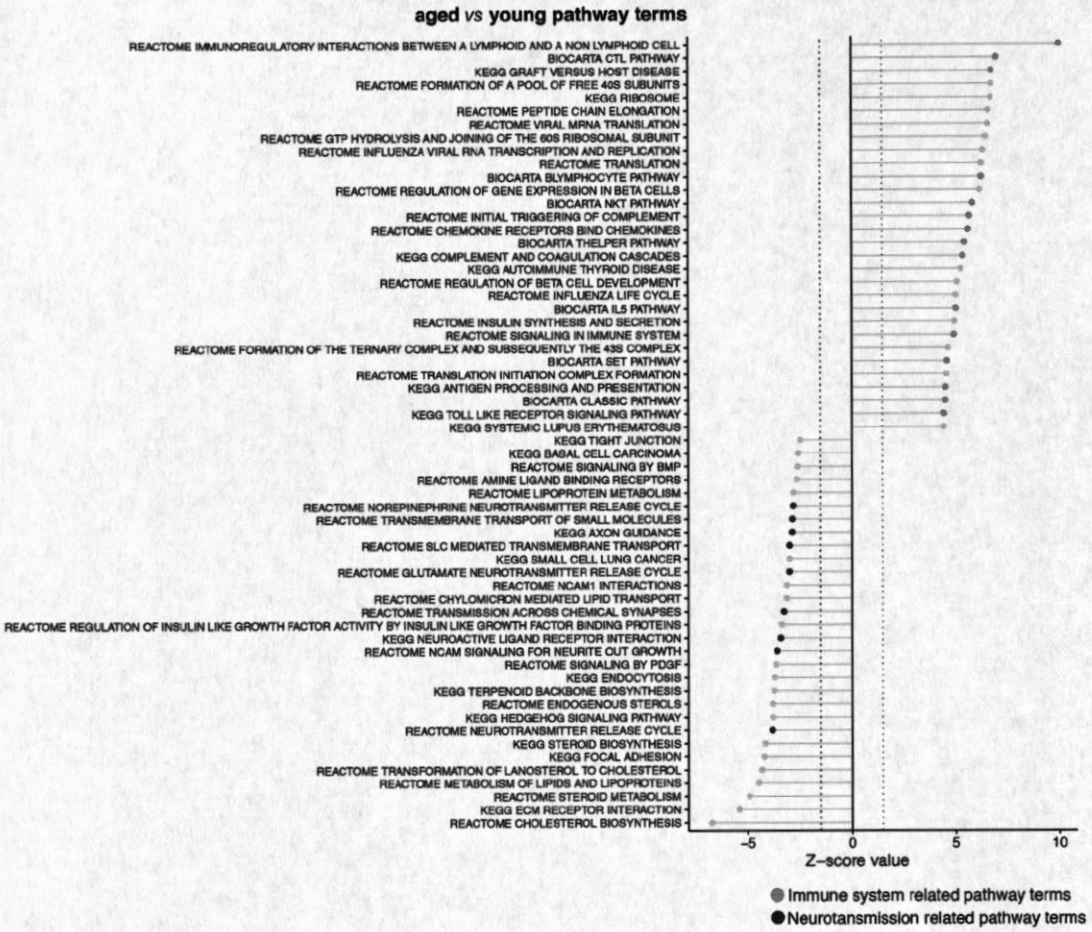

Fig. 8. Immune system- and neurotransmission-related pathway terms identified in aged vs. young RVLM pathway analysis. Horizontal line segment plot of significant top 30 ± Z-score pathway terms identified in aged vs. young RVLM GSEA. Pathway terms with PAGE Z-score <-1.5 or >1.5 (dotted reference lines on plots) and with P values <0.05 were considered as significant. Immune system-related pathway terms line segment ends were marked with red circles, and neurotransmission-related pathway terms line segment ends were marked with blue circles. The sample size for young and aged RVLM groups $n = 3$.

were observed between microarray and qPCR with higher correlation in aged vs. young comparison fold change values (r^2- 0.919) followed by aged vs. middle-aged and middle-aged vs. young RVLM comparisons (Fig. 13).

DISCUSSION

The goals of this study were to characterize the transcriptomic profile of the aging RVLM and to test the hypothesis that aging is associated with altered gene expression in the RVLM with an emphasis on immune system associated gene transcripts. The current results support this hypothesis in a number of important ways. First, the RVLM gene expression profile varied with age, and age-related RVLM gene expression changes were often characterized by progressive changes associated with chronological age. For example, higher numbers of DE genes were identified in aged vs. young comparison than in middle-aged vs. young comparison. Second, the expression of immune- and stress response-related genes was increased in the RVLM of aged compared with young and middle-aged rats. Age-related upregulation of immune- and stress response-associated GO and pathway sets, coupled with independent qPCR validation of selected immune response genes, supports this interpretation. Third, a decrease in the expression of genes associated with lipid metabolism, molecular transport, and chemical neurotransmission was identified in the aged RVLM. Fourth, the majority of RVLM chemical neurotransmission-related GO and pathway sets were significantly different in aged vs. middle-aged and aged vs. young RVLM comparisons yet were absent in the middle-aged vs. young comparison.

Brain aging is a complex process, and age-associated alterations contribute to central nervous system dysfunction (61). Deciphering cellular and molecular mechanisms associated with brain aging is essential for understanding age-dependent mental and physiological disorders, and a primary experimental step in this discovery process involves comparing brain gene expression patterns in young and aged brains (20). The results of studies using high-throughput analyses of brain tissue have identified age-related nonuniform changes in gene expression between separate brain areas, suggesting brain areas may age differently (18, 20, 23, 32). The approach used in the current study of combining micropunching with microarray-based, high-throughput analyses provided a strategy for determining if the RVLM-containing hindbrain area is characterized by age-related changes in gene expression.

Consistent with the results of previous studies focused on understanding the effects of aging on gene expression in the

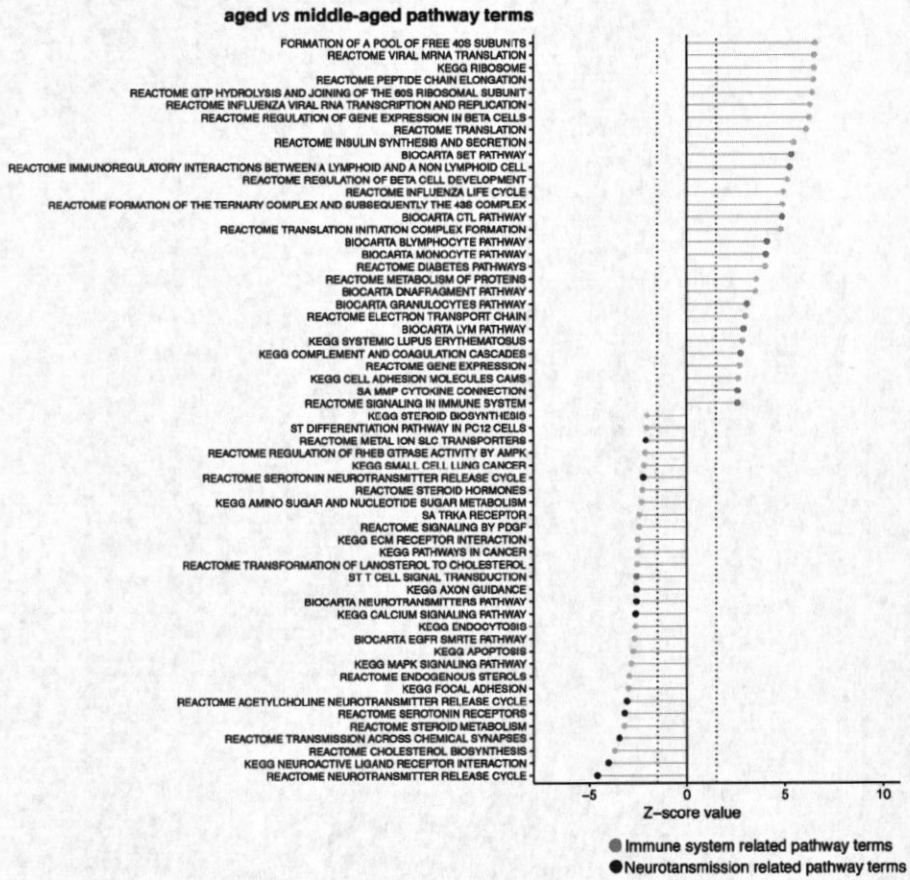

Fig. 9. Immune system- and neurotransmission-related pathway terms identified in aged vs. middle-aged RVLM pathway analysis. Horizontal line segment plot of significant top 30 ± Z-score pathway terms identified in aged vs. middle-aged RVLM GSEA. Pathway terms with PAGE Z-score <-1.5 or >1.5 (dotted reference lines on plots) and with P values <0.05 were considered as significant. Immune system-related pathway terms line segment ends were marked with red circles, and neurotransmission-related pathway terms line segment ends were marked with blue circles. The sample size for middle-aged and aged RVLM groups $n = 3$.

brain (6, 23, 32, 39, 48, 57, 60), the present findings indicate that immune response-associated genes and pathways were upregulated with advancing age (Table 2). Specifically, the complement cascade and several activation-related genes, including *C1qa*, *C1qb*, *C1qg*, *C3*, *C4a*, *Cfd*, *Cfh*, *Vwf*, and *Klkb1*, were upregulated significantly in the aged RVLM, and complement-related GO and pathway terms were significant in the RVLM of middle-aged and aged rats compared with young rats. The contribution of the complement cascade in synaptic remodeling in the developing brain is well established (52, 53, 62). On the other hand, the role of complement-mediated modulation in the adult brain is not well understood despite the fact that in response to injury or inflammation adult brain areas produce complement proteins (40, 52). It may be that increased expression of complement proteins and their activation contribute to the remodeling of RVLM-residing synaptic connections during aging, leading to alterations in RVLM-enriched sympathetic premotor neuron activity. In support of this notion, genes related to extracellular matrix degradation through activation of matrix metalloproteinases, which is necessary for synaptic structural remodeling (22), such as *Mmp14*, *Timp1*, *Timp2*, *Serpinh1*, and *Col5a3*, were altered in the RVLM of aged rats. Immune system cellular signaling pathways that play a role in mediating extracellular matrix degradation and synaptic remodeling, such as receptor-mediated phagocytosis and antigen presentation were upregulated in the RVLM of middle-aged and aged rats. Specifically, central nervous system (CNS) resident microglial cells and their activation-related genes, including *Cd14*, *Cd68*, *Tlr2*, *Cx3cr1*, *Trem2*, *Msr2*, and *B2m*, and toll-like receptor signaling pathways, were upregulated in the RVLM of aged rats, consistent with the presence of activated microglial cells known to be present in aged brains (40). Activation of microglia in the RVLM has been observed in rats with heart failure (15), a syndrome in which abnormal sympathoexcitation plays a critical role. Although, it is not clear how activated microglia influence RVLM functionality, Dworak et al. (15) observed a relationship between activated microglia and neuronal activation in the RVLM of heart failure rats. Similar mechanisms might be occurring in the aged RVLM, and studies focused on the influence of activated microglia on the functionality of neurons in the aged RVLM are needed to confirm this hypothesis. In concert, it is plausible to speculate that activated microglial cells and the complement system might modulate synaptic structural connectivity in the aging RVLM.

In addition to innate inflammatory response-related elements, an upregulation of adaptive immune T and B cell pathways was observed in the RVLM of middle-aged and aged rats (Table 2). Peripheral lymphocytes are not typically present in the brain because of the protective nature of the blood-brain barrier (BBB), which restricts the migration of peripheral cells and transport of molecules into the brain parenchyma (4, 16, 19). Although aging-associated alterations in BBB functions have been observed, such as increased permeability and transport (3, 7, 19, 51), there was a lack of evidence for an age-dependent increase in the infiltration of lymphocytes into

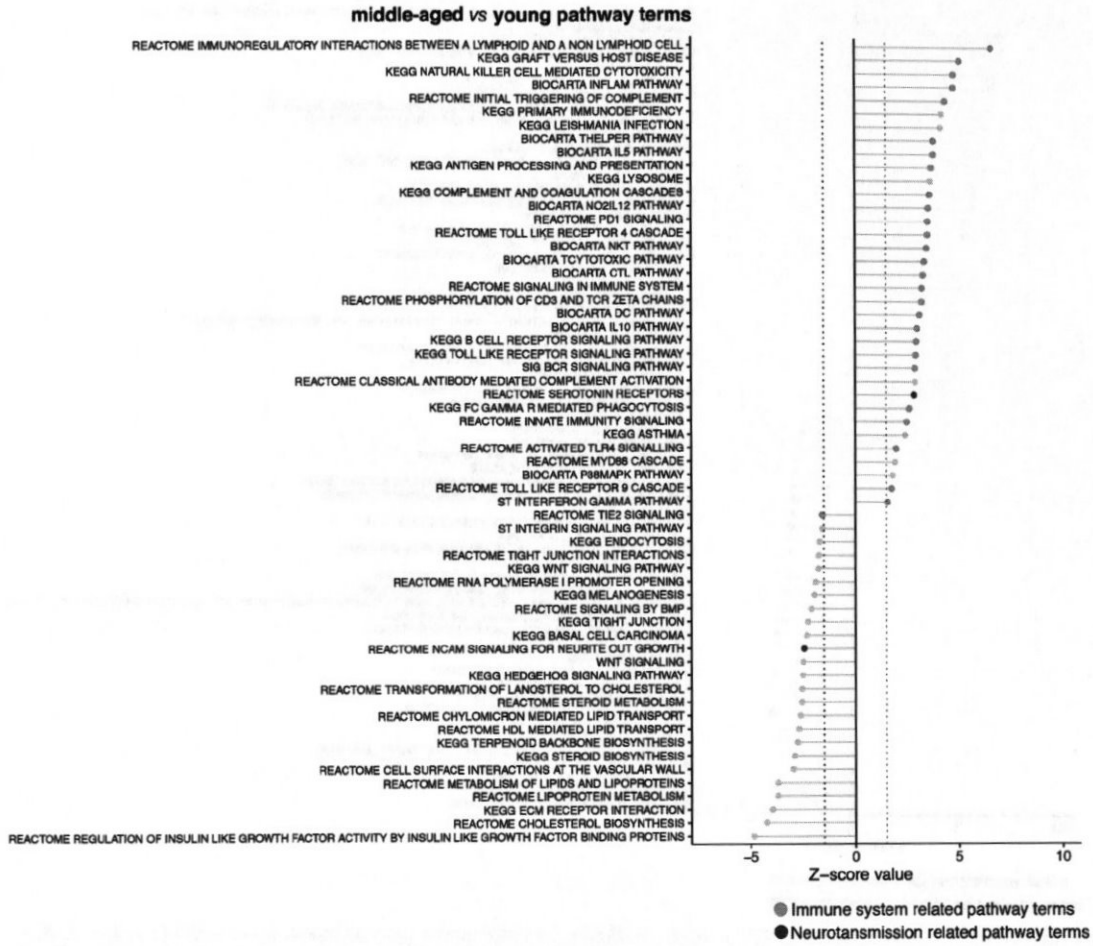

Fig. 10. Immune system- and neurotransmission-related pathway terms identified in middle-aged vs. young RVLM pathway analysis. Horizontal line segment plot of significant top 30 ± Z-score pathway terms identified in aged vs. middle-aged RVLM GSEA. Pathway terms with PAGE Z-score <-1.5 or >1.5 (dotted reference lines on plots) and with P values <0.05 were considered as significant. Immune system-related pathway terms line segment ends were marked with red circles, and neurotransmission-related pathway terms line segment ends were marked with blue circles. The sample size for young and middle-aged RVLM groups $n = 3$.

the brain parenchyma (19). It is possible that inflammatory responses mediated via cytokines in the aged RVLM might be causing infiltration of peripheral immune cells into this brainstem region. In support of this notion, gene sets that might be associated with altering BBB permeability, such as tight junctions and those for the extracellular matrix (19), were downregulated in middle-aged and aged RVLM. It is unclear how infiltrated lymphocytes may affect RVLM functionality, although it is worth speculating that reorganization of extracellular matrix in the RVLM may directly affect synaptic connectivity between RVLM neurons. Further studies are required to confirm infiltration of peripheral immune cells into the RVLM of aged rats, as well as the hypothesis that an age-dependent activated immune system may mediate RVLM synaptic remodeling.

The RVLM was also characterized by age-related alterations in genes involved with lipid metabolism and transport, especially cholesterol biosynthesis. Gene expression analysis of the hippocampus previously identified upregulation of cholesterol biosynthesis- associated genes in aged rats, suggesting an age-dependent increase in cholesterol metabolism (6). However, it has been speculated that aging-associated alterations in cholesterol biosynthesis might depend on brain region (41, 63). Contrary to age-dependent increased lipid biosynthesis, we found cholesterol synthesis-associated genes (41) (*Hmgcs1*, *Hmgcr*, and *Dhcr7*) and their respective pathways to be downregulated. Concomitantly, we observed the *Abca1* gene, which is involved in cholesterol efflux (30, 41), to be upregulated in the RVLM of middle-aged and aged rats compared with young rats (Table 2, Fig. 11). Taken together, these data suggest that cholesterol turnover may be decreasing in the RVLM of middle-aged and aged rats. The membrane component of cholesterol plays an essential role in insulating axons through myelination, maintaining ion-balance, and supporting dendritic and synaptic connectivity (41). Alterations in cholesterol homeostasis may affect neurotransmission in the RVLM, and it has been suggested previously that demyelination might cause immune responses in CNS (6). In agreement with this idea, gene sets associated with synapses, synaptic vesicles, and the postsynaptic membrane were downregulated, and as previously discussed, immune response-related genes were upregulated in the RVLM of aged rats.

Collectively, age-related changes in immune response- and lipid metabolism-related gene expression support the hypoth-

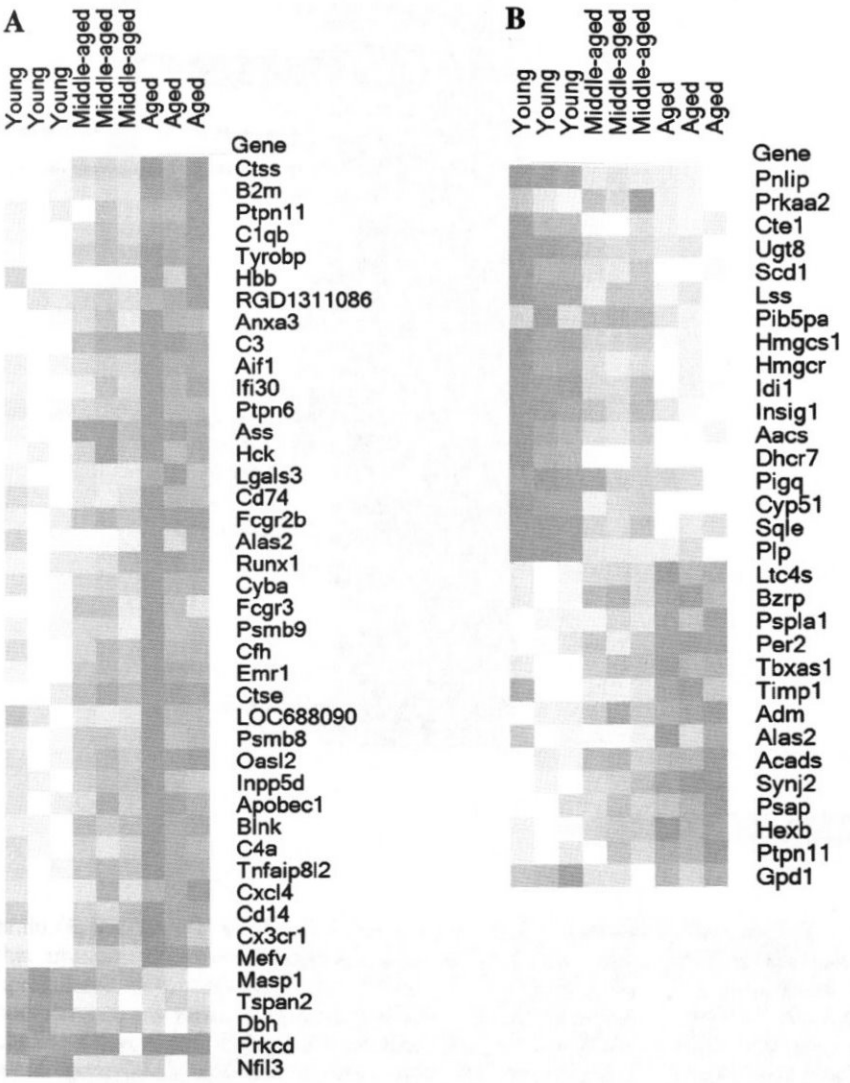

Fig. 11. Immune system (*A*) and lipid biosynthesis (*B*) associated DE genes sorted from Fig. 2*C* global analysis and their expression levels represented as a heat map matrix. The Z-score value for each gene was used as a parameter for its expression level. White cells indicate age-related low expression, and red cells indicate age-related high expression. To better represent each gene's altered expression, the heat map was constructed using row (each gene) normalization instead of data set normalization.

esis of age-dependent synaptic remodeling in the RVLM of middle-aged and aged rats. However, alterations in chemical neurotransmission-associated pathways were observed only in the RVLM of aged rats and were not altered in middle-aged rats (Table 2). These data suggest that primary changes in synaptic neurotransmission between RVLM neurons and/or between RVLM and other central sympathetic components might be occurring in F344 rats after middle age. Consistent with this idea, Kenney and Fels (26) reported previously that the reduced responsiveness of renal and splanchnic sympathetic nerve discharge (SND) to heat stress, which depends on the functional integrity of RVLM, was more pronounced in aged compared with middle-aged F344 rats (24–27). Studies focused on RVLM neurotransmission-associated gene and protein expression patterns are needed to confirm this hypothesis.

There are several methodological and analytical limitations in the current study that need to be acknowledged. First, although care was taken to use both stereotaxic and histological reference information to identify the RVLM as being within our sampled tissue, we cannot exclude the possibility that micropunches collected to analyze RVLM gene expression may have contained some tissue from areas surrounding the RVLM. However, several techniques were used to minimize this potential issue. First, we used an a priori approach to measure, on the basis of inferred stereotaxic space (28), the rostral boundary of the RVLM as delineated by the stereotaxic rat brain atlas of Paxinos and Watson (47). This involved identification of a known, easily identifiable cerebellar landmark within our tissue, matching its location to the correct rostrocaudal level in the atlas, and then using this level as the starting point to use our cryostat as a measuring device to count off a fixed number of sections of known thickness until the predicted stereotaxic location of the RVLM's rostral boundary emerged. Second, we used an a posteriori approach to confirm both the accuracy of our a priori approach and our sampling technique. This was achieved by microscopic and photomicrographic confirmation of landmarks on a cresyl violet-stained tissue section rostral to the micropunched sections and again on unstained micropunched sections. As predicted by the histological documentation provided by Paxinos and Watson (47), our micropunches sampled the rostral portion of the RVLM shortly after it appears in the tissue just ventral to the nucleus ambiguus, and at a level just caudal to the level where the facial nucleus last appears. Third, we used a tissue micropunch

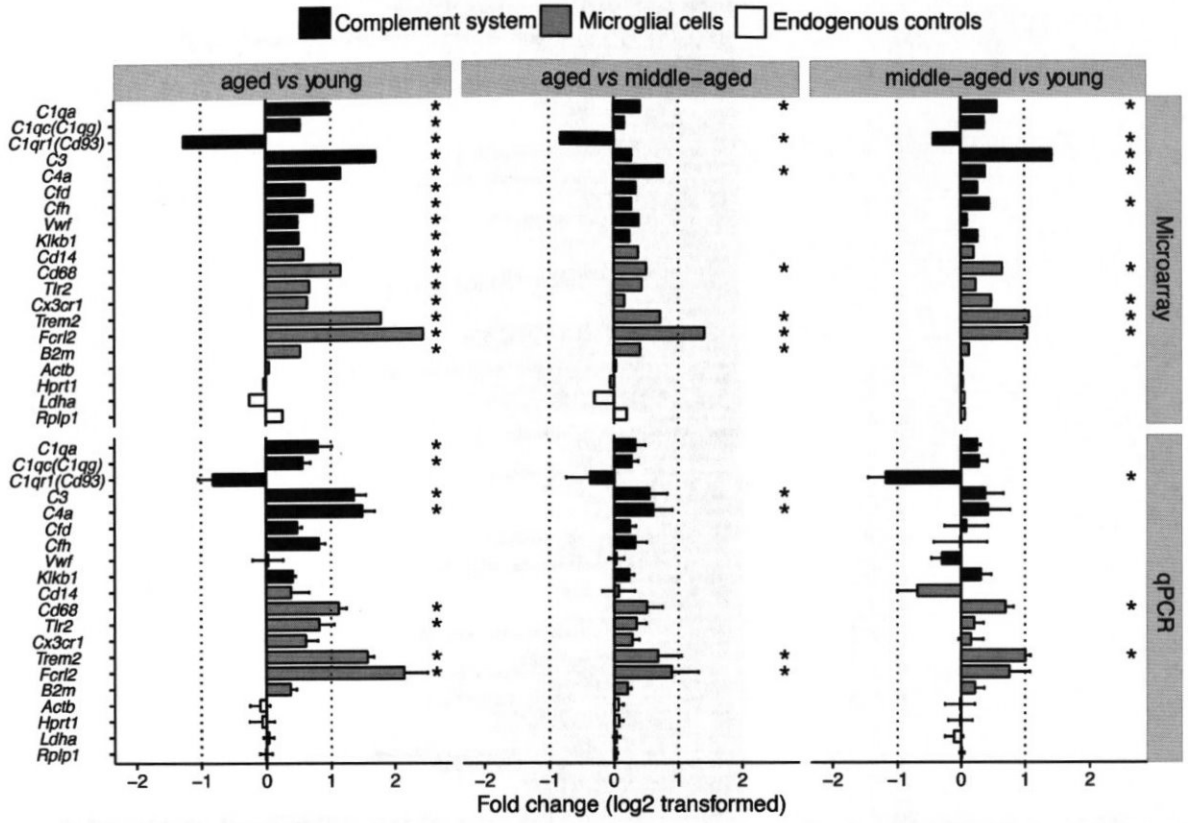

Fig. 12. quantitative (q)PCR validation of microarray identified immune system-associated genes differential expression in aging RVLM. Relative gene expression differences observed in microarray (*top* rows) and qPCR (*bottom* rows) in aged vs. young, aged vs. middle-aged, and middle-aged vs. young RVLM comparisons are represented as fold change value bar plots. Statistically significant genes are annotated with asterisk, and ± 2-fold change in gene expression is marked with vertical dotted lines. The sample size for young, middle-aged, and aged RVLM group $n = 5$. Statistical criteria for significant differentially expressed genes identified in microarray analysis: ANOVA<0.05, multiple-comparison Z-ratio <-1.5 or >1.5, Z-statistic P value <0.05, FDR <0.3, and probe signal intensity >0. Statistical criteria for significant DE genes identified in qPCR analysis: ANOVA P value <0.05, Benjamini-Hochberg FDR <0.1, and least significant difference post hoc test P value <0.05.

instrument of relatively small inner diameter (0.5 mm) to ensure that we discretely sampled tissue within the confines of the RVLM. Finally, to further validate our results, we used several replicates of micropunches from each group for microarray and qPCR analyses. Collectively, these approaches provide converging evidence that the RVLM was sampled accurately and enriched within our micropunched samples.

A second limitation, in traditional terms, was that the sample size used in the present investigation for our microarray method was from relatively few subjects. However, because of the difficulty in integrating error rates associated with the identification of DE genes and with gene class testing (for example GO and pathway analysis), there is no clear consensus on gold-standard methods used for sample size and power

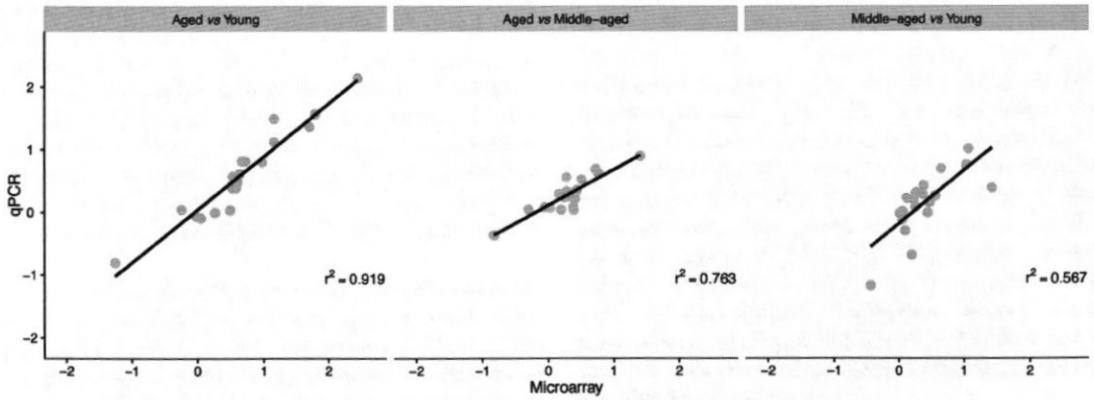

Fig. 13. Consistency of gene expression fold change (log2 transformed) values observed in aged vs. young, aged vs. middle-aged and middle-aged vs. young RVLM comparisons between microarray (x-axis) and qPCR (y-axis) represented with scatter plots. Each analyzed gene is depicted as a gray-colored filled circle, and each comparison coefficient of determination (r^2) values are annotated on the graph.

Table 2. *Comprehensive view of age-dependent altered molecular mechanisms in the RVLM*

Aged vs. Young RVLM	Aged vs. Middle-aged RVLM	Middle-aged vs. Young RVLM
↑ Immune response	**↑ Immune response**	**↑ Immune response**
Complement cascade	Complement cascade	Complement cascade
Antigen presentation	Antigen presentation	Antigen presentation
B and T cell pathways	B cell and monocyte pathways	B cell and monocyte pathways
↑ Stress response	**↑ Stress response**	
DNA damage response	DNA damage response	
Mitochondrial metabolism	Mitochondrial metabolism	
↑ Protein metabolism	**↑ Protein metabolism**	
Translational machinery	Translational machinery	
Protein folding and degradation	Protein folding and degradation	
↓ Lipid metabolism	**↓ Lipid metabolism**	**↓ Lipid metabolism**
Cholesterol and steroid biosynthesis and transport	Cholesterol and steroid biosynthesis and transport	Cholesterol and steroid biosynthesis and transport
↓ Neurotransmission	**↓ Neurotransmission**	
Neurotransmitter metabolism and release cycle	Neurotransmitter metabolism and release cycle	
Small molecule and ion transport	Small molecule transport	
Synaptic plasticity	Synaptic plasticity	

Shown are synthesized coherent mechanisms that were significantly changed with aging in the RVLM. Each broader mechanism (boldface) and its subcategories (lightface) summarized were constructed from aged vs. young, aged vs. middle-aged and middle-aged vs. young RVLM Gene Ontology (GO) and pathway analysis. ↑ indicates upregulation, and ↓ indicates downregulation of associated gene expression.

estimation for microarrays, especially those involving small amounts of brain tissue. Therefore, instead of drawing inferences from only DE genes, we opted to use whole microarray data sets for GSEA analysis, an analytical method that has been suggested to increase the power to detect overall differential expression in a microarray study (2).

Third, false positives are intrinsic to microarray PAGE-based GSEA analysis. However, the use of FDR correction in gene set analysis, consistency of the findings with previously published aging brain studies, and correlation of chronological SND alterations with RVLM gene expression rectify this potential problem. In addition, the increase in immune response-related transcripts in the aging RVLM was validated by qPCR. Although much of the discussion was drawn from overrepresentation analysis, multidimensional reasoning was also used to discuss possible age-dependent, immune system-mediated alterations in synaptic connections. Finally, gene expression changes may not always correlate with protein changes (33, 59), and it is necessary to test and confirm the hypotheses proposed in the current study at the protein and cellular levels to identify age-dependent mechanisms that might be altering the functionality of the RVLM.

In conclusion, the present study is the first to characterize and compare the transcriptomic profiles of the RVLM in young, middle-aged, and aged F344 rats. The global changes we observed in gene expression patterns in the entire RVLM suggest that aging might alter gene expression in this region in a manner that cuts across multiple cell types and subregions of the RVLM and provide an experimental strategy to identify key molecular mechanisms underpinning age-dependent changes in physiological regulation within the diverse systems served by the RVLM. The current results suggest that the aged RVLM is characterized by increased immune response-associated transcripts and alterations in neural-immune interactions, and further studies of specific neural substrates and neuronal populations within the RVLM may reveal systems-level alterations in gene expression patterns that are perhaps both more discrete and differentiated.

GRANTS

This study was supported by National Institute on Aging Grant AG-041948 and the Intramural Research Program of the National Institute of Aging (National Institutes of Health).

DISCLOSURES

Authors declare no conflicts of interest.

AUTHOR CONTRIBUTIONS

S.B., C.K.G., Y.Z., and R.J.O. performed experiments; S.B. and Y.Z. analyzed data; S.B. and Y.Z. interpreted results of experiments; S.B. prepared figures; S.B. drafted manuscript; S.B., C.K.G., H.N.P., A.M.K., and M.J.K. edited and revised manuscript; S.B., C.K.G., Y.Z., H.N.P., R.J.O., K.G.B., A.M.K., and M.J.K. approved final version of manuscript; C.K.G., K.G.B., and M.J.K. conceived and designed research.

REFERENCES

1. **Abdelnour A.** MIQE compliant qPCR data analysis and statistics. In: *MIQE & qPCR: How to Apply the MIQE Guidelines - a Visual, Interactive and Practical qPCR Guide*, DOOMS Editions, 2016.
2. **Allison DB, Cui X, Page GP, Sabripour M.** Microarray data analysis: from disarray to consolidation and consensus. *Nat Rev Genet* 7: 55–65, 2006. doi:10.1038/nrg1749.
3. **Bake S, Friedman JA, Sohrabji F.** Reproductive age-related changes in the blood brain barrier: expression of IgG and tight junction proteins. *Microvasc Res* 78: 413–424, 2009. doi:10.1016/j.mvr.2009.06.009.
4. **Bechmann I, Galea I, Perry VH.** What is the blood-brain barrier (not)? *Trends Immunol* 28: 5–11, 2007. doi:10.1016/j.it.2006.11.007.
5. **Benarroch EE, Schmeichel AM, Parisi JE, Low PA.** Putative neuropathological interactions in MSA: focus in the rostral ventrolateral medulla. *Clin Auton Res* 25: 77–80, 2015. doi:10.1007/s10286-015-0273-2.
6. **Blalock EM, Chen KC, Sharrow K, Herman JP, Porter NM, Foster TC, Landfield PW.** Gene microarrays in hippocampal aging: statistical profiling identifies novel processes correlated with cognitive impairment. *J Neurosci* 23: 3807–3819, 2003.
7. **Blau CW, Cowley TR, O'Sullivan J, Grehan B, Browne TC, Kelly L, Birch A, Murphy N, Kelly AM, Kerskens CM, Lynch MA.** The age-related deficit in LTP is associated with changes in perfusion and blood-brain barrier permeability. *Neurobiol Aging* 33: e23–e35, 2012. doi:10.1016/j.neurobiolaging.2011.09.035.
8. **Blessing WW.** *The Lower Brainstem and Bodily Homeostasis*. New York, Oxford: Oxford University Press, 1997, p. xiv.
9. **Card JP, Kobiler O, McCambridge J, Ebdlahad S, Shan Z, Raizada MK, Sved AF, Enquist LW.** Microdissection of neural networks by

conditional reporter expression from a Brainbow herpesvirus. *Proc Natl Acad Sci USA* 108: 3377–3382, 2011. doi:10.1073/pnas.1015033108.

10. **Card JP, Sved JC, Craig B, Raizada M, Vazquez J, Sved AF.** Efferent projections of rat rostroventrolateral medulla C1 catecholamine neurons: Implications for the central control of cardiovascular regulation. *J Comp Neurol* 499: 840–859, 2006. doi:10.1002/cne.21140.
11. **Cersosimo MG, Benarroch EE.** Central control of autonomic function and involvement in neurodegenerative disorders. *Handb Clin Neurol* 117: 45–57, 2013. doi:10.1016/B978-0-444-53491-0.00005-5.
12. **Cheadle C, Vawter MP, Freed WJ, Becker KG.** Analysis of microarray data using Z score transformation. *J Mol Diagn* 5: 73–81, 2003. doi:10.1016/S1525-1578(10)60455-2.
13. **De S, Zhang Y, Garner JR, Wang SA, Becker KG.** Disease and phenotype gene set analysis of disease-based gene expression in mouse and human. *Physiol Genomics* 42A: 162–167, 2010. doi:10.1152/physiolgenomics.00008.2010.
14. **Dempsey B, Le S, Turner A, Bokiniec P, Ramadas R, Bjaalie JG, Menuet C, Neve R, Allen AM, Goodchild AK, McMullan S.** Mapping and analysis of the connectome of sympathetic premotor neurons in the rostral ventrolateral medulla of the rat using a volumetric brain atlas. *Front Neural Circuits* 11: 9, 2017. doi:10.3389/fncir.2017.00009.
15. **Dworak M, Stebbing M, Kompa AR, Rana I, Krum H, Badoer E.** Attenuation of microglial and neuronal activation in the brain by ICV minocycline following myocardial infarction. *Auton Neurosci* 185: 43–50, 2014. doi:10.1016/j.autneu.2014.03.007.
16. **Engelhardt B, Sorokin L.** The blood-brain and the blood-cerebrospinal fluid barriers: function and dysfunction. *Semin Immunopathol* 31: 497–511, 2009. doi:10.1007/s00281-009-0177-0.
17. **Erraji-Benchekroun L, Underwood MD, Arango V, Galfalvy H, Pavlidis P, Smyrniotopoulos P, Mann JJ, Sibille E.** Molecular aging in human prefrontal cortex is selective and continuous throughout adult life. *Biol Psychiatry* 57: 549–558, 2005. doi:10.1016/j.biopsych.2004.10.034.
18. **Fraser HB, Khaitovich P, Plotkin JB, Pääbo S, Eisen MB.** Aging and gene expression in the primate brain. *PLoS Biol* 3: e274, 2005. doi:10.1371/journal.pbio.0030274.
19. **Gemechu JM, Bentivoglio M.** T Cell Recruitment in the Brain during Normal Aging. *Front Cell Neurosci* 6: 38, 2012. doi:10.3389/fncel.2012.00038.
20. **Ginsberg SD.** Expression profile analysis of brain aging, in *Brain Aging: Models, Methods, and Mechanisms*, edited by Riddle DR. Boca Raton, FL: CRC Press/Taylor & Francis, 2007. doi:10.1201/9781420005523.ch7.
21. **Helwig BG, Parimi S, Ganta CK, Cober R, Fels RJ, Kenney MJ.** Aging alters regulation of visceral sympathetic nerve responses to acute hypothermia. *Am J Physiol Regul Integr Comp Physiol* 291: R573–R579, 2006. doi:10.1152/ajpregu.00903.2005.
22. **Huntley GW.** Synaptic circuit remodelling by matrix metalloproteinases in health and disease. *Nat Rev Neurosci* 13: 743–757, 2012. doi:10.1038/nrn3320.
23. **Jiang CH, Tsien JZ, Schultz PG, Hu Y.** The effects of aging on gene expression in the hypothalamus and cortex of mice. *Proc Natl Acad Sci USA* 98: 1930–1934, 2001. doi:10.1073/pnas.98.4.1930.
24. **Kenney MJ.** Animal aging and regulation of sympathetic nerve discharge. *J Appl Physiol (1985)* 109: 951–958, 2010. doi:10.1152/japplphysiol.00506.2010.
25. **Kenney MJ.** Medullary regulation of visceral sympathetic nerve discharge at peak hyperthermia in aged F344 rats. *Auton Neurosci* 186: 32–37, 2014. doi:10.1016/j.autneu.2014.09.003.
26. **Kenney MJ, Fels RJ.** Sympathetic nerve regulation to heating is altered in senescent rats. *Am J Physiol Regul Integr Comp Physiol* 283: R513–R520, 2002. doi:10.1152/ajpregu.00683.2001.
27. **Kenney MJ, Meyer CN, Hosking KG, Fels RJ.** Is visceral sympathoexcitation to heat stress dependent on activation of ionotropic excitatory amino acid receptors in the rostral ventrolateral medulla? *Am J Physiol Regul Integr Comp Physiol* 301: R548–R557, 2011. doi:10.1152/ajpregu.00113.2011.
28. **Khan AM.** Controlling feeding behavior by chemical or gene-directed targeting in the brain: what's so spatial about our methods? *Front Neurosci* 7: 182, 2013. doi:10.3389/fnins.2013.00182.
29. **Kim SY, Volsky DJ.** PAGE: parametric analysis of gene set enrichment. *BMC Bioinformatics* 6: 144, 2005. doi:10.1186/1471-2105-6-144.
30. **Kim WS, Rahmanto AS, Kamili A, Rye KA, Guillemin GJ, Gelissen IC, Jessup W, Hill AF, Garner B.** Role of ABCG1 and ABCA1 in regulation of neuronal cholesterol efflux to apolipoprotein E discs and suppression of amyloid-beta peptide generation. *J Biol Chem* 282: 2851–2861, 2007. doi:10.1074/jbc.M607831200.
31. **King JY, Ferrara R, Tabibiazar R, Spin JM, Chen MM, Kuchinsky A, Vailaya A, Kincaid R, Tsalenko A, Deng DX, Connolly A, Zhang P, Yang E, Watt C, Yakhini Z, Ben-Dor A, Adler A, Bruhn L, Tsao P, Quertermous T, Ashley EA.** Pathway analysis of coronary atherosclerosis. *Physiol Genomics* 23: 103–118, 2005. doi:10.1152/physiolgenomics.00101.2005.
32. **Lee C-K, Weindruch R, Prolla TA.** Gene-expression profile of the ageing brain in mice. *Nat Genet* 25: 294–297, 2000. doi:10.1038/77046.
33. **Lewandowski NM, Small SA.** Brain microarray: finding needles in molecular haystacks. *J Neurosci* 25: 10341–10346, 2005. doi:10.1523/JNEUROSCI.4006-05.2005.
34. **Lipski J, Kanjhan R, Kruszewska B, Rong WF, Smith M.** Presympathetic neurones in the rostral ventrolateral medulla of the rat: electrophysiology, morphology and relationship to adjacent neuronal groups. *Acta Neurobiol Exp (Wars)* 56: 373–384, 1996.
35. **Lipski J, Kanjhan R, Kruszewska B, Smith M.** Barosensitive neurons in the rostral ventrolateral medulla of the rat in vivo: morphological properties and relationship to C1 adrenergic neurons. *Neuroscience* 69: 601–618, 1995. doi:10.1016/0306-4522(95)92652-Z.
36. **Livak KJ, Schmittgen TD.** Analysis of relative gene expression data using real-time quantitative PCR and the 2(-delta delta C(T)) method. *Methods* 25: 402–408, 2001. doi:10.1006/meth.2001.1262.
37. **Llewellyn-Smith IJ, Verberne AJM.** *Central Regulation of Autonomic Functions*. New York, Oxford: Oxford University Press, 2011, p. xv. doi:10.1093/acprof:oso/9780195306637.001.0001
38. **Loewy AD, Spyer KM.** *Central Regulation of Autonomic Functions*. New York, Oxford: Oxford University Press, 1990, p. xii.
39. **Lu T, Pan Y, Kao SY, Li C, Kohane I, Chan J, Yankner BA.** Gene regulation and DNA damage in the ageing human brain. *Nature* 429: 883–891, 2004. doi:10.1038/nature02661.
40. **Lucin KM, Wyss-Coray T.** Immune activation in brain aging and neurodegeneration: too much or too little? *Neuron* 64: 110–122, 2009. doi:10.1016/j.neuron.2009.08.039.
41. **Martin M, Dotti CG, Ledesma MD.** Brain cholesterol in normal and pathological aging. *Biochim Biophys Acta* 1801: 934–944, 2010. doi:10.1016/j.bbalip.2010.03.011.
42. **Mitchell SJ, Scheibye-Knudsen M, Longo DL, de Cabo R.** Animal models of aging research: implications for human aging and age-related diseases. *Annu Rev Anim Biosci* 3: 283–303, 2015. doi:10.1146/annurev-animal-022114-110829.
43. **Nolan PC, Waldrop TG.** Ventrolateral medullary neurons show age-dependent depolarizations to hypoxia in vitro. *Brain Res Dev Brain Res* 91: 111–120, 1996. doi:10.1016/0165-3806(95)00166-2.
44. **Oliveros JC, Venny.** An interactive tool for comparing lists with Venn's diagrams. http://bioinfogp.cnb.csic.es/tools/venny/index.html.
45. **Palkovits M.** Microdissection of individual brain nuclei and areas. In: *General Neurochemical Techniques*, edited by Boulton AA, Baker GB. Clifton, NJ: Humana, 1986, p. 1–17.
46. **Palkovits M, Jacobowitz DM.** Topographic atlas of catecholamine and acetylcholinesterase-containing neurons in the rat brain. II. Hindbrain (mesencephalon, rhombencephalon). *J Comp Neurol* 157: 29–42, 1974. doi:10.1002/cne.901570104.
47. **Paxinos G, Watson C.** *The Rat Brain in Stereotaxic Coordinates*. London: Academic, 2014.
48. **Prolla TA.** DNA microarray analysis of the aging brain. *Chem Senses* 27: 299–306, 2002. doi:10.1093/chemse/27.3.299.
49. **Ramón y Cajal S.** *Texture of the Nervous System of Man and the Vertebrates*. Wien: Springer, 2000. doi:10.1007/978-3-7091-6315-3.
50. **Schreihofer AM, Sved AF.** The ventrolateral medulla and sympathetic regulation of arterial pressure, in *Central Regulation of Autonomic Functions*. New York, Oxford: Oxford University Press, 2011, p. 78–97. doi:10.1093/acprof:oso/9780195306637.003.0005.
51. **Shah GN, Mooradian AD.** Age-related changes in the blood-brain barrier. *Exp Gerontol* 32: 501–519, 1997. doi:10.1016/S0531-5565(96)00158-1.
52. **Stephan AH, Barres BA, Stevens B.** The complement system: an unexpected role in synaptic pruning during development and disease. *Annu Rev Neurosci* 35: 369–389, 2012. doi:10.1146/annurev-neuro-061010-113810.
53. **Stevens B, Allen NJ, Vazquez LE, Howell GR, Christopherson KS, Nouri N, Micheva KD, Mehalow AK, Huberman AD, Stafford B, Sher A, Litke AM, Lambris JD, Smith SJ, John SW, Barres BA.** The

classical complement cascade mediates CNS synapse elimination. *Cell* 131: 1164–1178, 2007. doi:10.1016/j.cell.2007.10.036.

54. **Stornetta RL.** Neurochemistry of bulbospinal presympathetic neurons of the medulla oblongata. *J Chem Neuroanat* 38: 222–230, 2009. doi:10.1016/j.jchemneu.2009.07.005.
55. **Subramanian M, Hahn-Townsend C, Clark KA, MohanKumar SM, MohanKumar PS.** Chronic estrogen exposure affects gene expression in the rostral ventrolateral medulla of young and aging rats: possible role in hypertension. *Brain Res* 1627: 134–142, 2015. doi:10.1016/j.brainres.2015.09.007.
56. **Tusher VG, Tibshirani R, Chu G.** Significance analysis of microarrays applied to the ionizing radiation response. *Proc Natl Acad Sci USA* 98: 5116–5121, 2001. doi:10.1073/pnas.091062498.
57. **Uddin RK, Singh SM.** Hippocampal gene expression meta-analysis identifies aging and age-associated spatial learning impairment (ASLI) genes and pathways. *PLoS One* 8: e69768, 2013. doi:10.1371/journal.pone.0069768.
58. **Verberne AJ, Sabetghadam A, Korim WS.** Neural pathways that control the glucose counterregulatory response. *Front Neurosci* 8: 38, 2014. doi:10.3389/fnins.2014.00038.
59. **Vogel C, Marcotte EM.** Insights into the regulation of protein abundance from proteomic and transcriptomic analyses. *Nat Rev Genet* 13: 227–232, 2012.
60. **Wood SH, Craig T, Li Y, Merry B, de Magalhães JP.** Whole transcriptome sequencing of the aging rat brain reveals dynamic RNA changes in the dark matter of the genome. *Age (Dordr)* 35: 763–776, 2013. doi:10.1007/s11357-012-9410-1.
61. **Yankner BA, Lu T, Loerch P.** The aging brain. *Annu Rev Pathol* 3: 41–66, 2008. doi:10.1146/annurev.pathmechdis.2.010506.092044.
62. **Zabel MK, Kirsch WM.** From development to dysfunction: microglia and the complement cascade in CNS homeostasis. *Ageing Res Rev* 12: 749–756, 2013. doi:10.1016/j.arr.2013.02.001.
63. **Zhang Y, Appelkvist EL, Kristensson K, Dallner G.** The lipid compositions of different regions of rat brain during development and aging. *Neurobiol Aging* 17: 869–875, 1996. doi:10.1016/S0197-4580(96)00076-0.
64. **Zucker IH, Xiao L, Haack KK.** The central renin-angiotensin system and sympathetic nerve activity in chronic heart failure. *Clin Sci (Lond)* 126: 695–706, 2014. doi:10.1042/CS20130294.